1-1-2017

A dual-chamber method for quantifying the effects of atmospheric perturbations on secondary organic aerosol formation from biomass burning emissions

Daniel S. Tkacik
Carnegie Mellon University

Ellis S. Robinson
Carnegie Mellon University

Adam Ahern
Carnegie Mellon University

Rawad Saleh
Carnegie Mellon University

Chelsea Stockwell
University of Montana

Recommended Citation

Authors

Daniel S. Tkacik, Ellis S. Robinson, Adam Ahern, Rawad Saleh, Chelsea Stockwell, Patrick Veres, Isobel J. Simpson, Simone Meinardi, Donald R. Blake, Robert J. Yokelson, Albert A. Presto, Ryan C. Sullivan, Neil M. Donahue, and Allen L. Robinson

RESEARCH ARTICLE

Key Points:
- Perturbing biomass burning (BB) emissions with UV, UV + HONO, and dark ozonolysis in a smog chamber creates secondary organic aerosol (SOA)
- The amount of SOA formation from biomass smoke is highly variable
- Burn-to-burn differences in the composition of BB emissions cause more variability in SOA production than different atmospheric perturbations

Supporting Information:
- Supporting Information S1

A dual-chamber method for quantifying the effects of atmospheric perturbations on secondary organic aerosol formation from biomass burning emissions

Daniel S. Tkacik[1] (iD), Ellis S. Robinson[1], Adam Ahern[1] (iD), Rawad Saleh[1] (iD), Chelsea Stockwell[2], Patrick Veres[3] (iD), Isobel J. Simpson[4], Simone Meinardi[4] (iD), Donald R. Blake[4] (iD), Robert J. Yokelson[2] (iD), Albert A. Presto[1] (iD), Ryan C. Sullivan[1] (iD), Neil M. Donahue[1] (iD), and Allen L. Robinson[1] (iD)

[1]Center for Atmospheric Particle Studies, Carnegie Mellon University, Pittsburgh, Pennsylvania, USA, [2]Department of Chemistry, University of Montana, Missoula, Montana, USA, [3]Chemical Sciences Division, Earth System Research Laboratory, National Oceanic and Atmospheric Administration, Boulder, Colorado, USA, [4]Department of Chemistry, University of California, Irvine, Irvine, California, USA

Abstract Biomass burning (BB) is a major source of atmospheric pollutants. Field and laboratory studies indicate that secondary organic aerosol (SOA) formation from BB emissions is highly variable. We investigated sources of this variability using a novel dual-smog-chamber method that directly compares the SOA formation from the same BB emissions under two different atmospheric conditions. During each experiment, we filled two identical Teflon smog chambers simultaneously with BB emissions from the same fire. We then perturbed the smoke with UV lights, UV lights plus nitrous acid (HONO), or dark ozone in one or both chambers. These perturbations caused SOA formation in nearly every experiment with an average organic aerosol (OA) mass enhancement ratio of 1.78 ± 0.91 (mean ± 1σ). However, the effects of the perturbations were highly variable ranging with OA mass enhancement ratios ranging from 0.7 (30% loss of OA mass) to 4.4 across the set of perturbation experiments. There was no apparent relationship between OA enhancement and perturbation type, fuel type, and modified combustion efficiency. To better isolate the effects of different perturbations, we report dual-chamber enhancement (DUCE), which is the quantity of the effects of a perturbation relative to a reference condition. DUCE values were also highly variable, even for the same perturbation and fuel type. Gas measurements indicate substantial burn-to-burn variability in the magnitude and composition of SOA precursor emissions, even in repeated burns of the same fuel under nominally identical conditions. Therefore, the effects of different atmospheric perturbations on SOA formation from BB emissions appear to be less important than burn-to-burn variability.

1. Introduction

Secondary organic aerosol (SOA) contributes a significant fraction of tropospheric fine-particle mass, but its sources and formation mechanisms are uncertain [*Kroll and Seinfeld*, 2008; *De Gouw and Jimenez*, 2009; *Hallquist et al.*, 2009]. SOA forms when atmospheric oxidation of gas-phase precursors creates low-volatility products, driving condensation to the particle phase. Combustion sources emit a complex mixture of SOA precursors, and the SOA formation from these emissions can vary widely [*Reid et al.*, 1998; *Robinson et al.*, 2007; *De Gouw and Jimenez*, 2009; *Grieshop et al.*, 2009; *Yokelson et al.*, 2009; *DeCarlo et al.*, 2010; *Cubison et al.*, 2011; *Hennigan et al.*, 2011; *Miracolo et al.*, 2011].

Biomass burning is a major source of atmospheric pollutants. SOA formation from biomass burning emissions appears to be especially complex. Field studies have shown both substantial production [*Lee et al.*, 2008; *Yokelson et al.*, 2009] and loss [*Reid et al.*, 1998; *DeCarlo et al.*, 2010; *Akagi et al.*, 2012; *Jolleys et al.*, 2012] of organic aerosol (OA) mass in biomass burning plumes. Similar variability has been observed in laboratory studies that photo-oxidized emissions in flow tubes [e.g., *Ortega et al.*, 2013] and smog chambers [*Hennigan et al.*, 2011].

The variability of SOA formation in fire plumes is not well understood. Many factors influence SOA formation, including precursor mixture, organic aerosol concentration, oxidant exposure, multiphase chemistry, temperature, relative humidity, and radical branching [*Hallquist et al.*, 2009]. In addition, biomass burning

emissions are extremely complex; even laboratory studies employing state-of-the-art instrumentation often can only speciate small fractions of the organic emissions at the molecular level [*Yokelson et al.*, 2013; *Hatch et al.*, 2015; *Stockwell et al.*, 2015]. Finally, the uncontrolled nature of fires means that the physiochemical composition of the biomass emissions varies from burn to burn, even with the same fuel and nominally identical conditions, making it difficult to isolate effects of different atmospheric perturbations, such as organic aerosol concentration or volatile organic compound (VOC)/NO_x (the mixing ratio of VOC to NO_x; ppbC/ppbNO$_x$). For example, *Hennigan et al.* [2011] reported a very wide range of SOA production from the photo-oxidation of biomass burning emissions in a laboratory smog chamber under various VOC/NO_x conditions. However, each smog chamber experiment used emissions from different burns, making it difficult to isolate the effects of atmospheric perturbations versus burn-to-burn differences in emission composition. To investigate the influence of atmospheric perturbations on SOA formation in biomass burning emissions, improved experimental methods are needed.

In this manuscript we describe an experimental study that systematically investigated the effects of different atmospheric perturbations on SOA formation from biomass burning emissions. During each experiment, we filled two identical smog chambers simultaneously with dilute emissions from the same biomass fire. We then perturbed one or both of the smog chambers and characterized the evolution of gas and particle phase organics. Since both chambers contained identical emissions, any relative difference in SOA production or change in OA properties between the two chambers was caused by the perturbation, not differences in emissions. We performed experiments systematically to investigate the effects of photo-oxidation, ozonolysis, and NO_x on SOA formation in biomass burning emissions from a number of fuels. Additional analysis of the High-Resolution Aerosol Mass Spectrometer (HR-AMS) data and SOA mass closure from fourth Fire Lab At Missoula Experiment (FLAME-IV) will be the focus of an upcoming study.

2. Experimental Section

We performed dual-chamber experiments during the fourth Fire Lab At Missoula Experiment (FLAME-IV) study at the Fire Science Laboratory (FSL) in Missoula, Montana in October–November 2012. Details of the FLAME-IV experiments are described by *Stockwell et al.*, 2015. The specific details of FSL's main combustion chamber, a 12.4 m × 12.4 m × 19.6 m room where biomass burns were conducted, are described elsewhere [*Yokelson et al.*, 1996; *Christian et al.*, 2003; *McMeeking et al.*, 2009; *Stockwell et al.*, 2015]. Table S2 in the supporting information lists the fuel, modified combustion efficiency, chamber conditions, and OA mass enhancements for each experiment.

2.1. Fuels and Burn Description

We produced biomass burning emissions from the combustion of seven vegetation types, performing multiple experiments with two fuels: ponderosa pine and black spruce. A complete list of experiments is shown in the supporting information. We chose ponderosa pine and black spruce as focus fuels because they are important North American wildland fuels and because their emissions showed very different OA mass enhancements during the FLAME-III campaign—a 10% net loss versus a 200% increase of OA mass for ponderosa pine and black spruce, respectively, when subjected to low-NO_x photo-oxidation [*Hennigan et al.*, 2011]. Experiments were also performed with ocote, hay, sawgrass, rice straw, and peat [*Stockwell et al.*, 2015].

Except for ocote, we conducted each burn by placing a small amount (0.5–2 kg) of fuel on a ceramic platform mounted on a scale that measured the mass of fuel consumed during a burn [*Stockwell et al.*, 2015]. In most cases we used electrical heating coils to ignite the fuel [*Hennigan et al.*, 2011]; in a few cases, we used a propane torch [*Stockwell et al.*, 2015]. The heating coil produces no emissions, while the propane torch produced a very small amount of emissions ($\ll$1% of mass of biomass burned) of primarily CO_2 with trace amounts of propane, CH_4, and C_2H_2 that should not influence the results of these experiments. The ocote was burned in two different types of cookstoves: an Envirofit Rocket G-3300 stove and a Philips HD4012 "gasifier" stove [*Stockwell et al.*, 2015].

Most fuels used in this study were relatively homogeneous to reduce sample-to-sample variation, but the coniferous fuels (e.g., black spruce and ponderosa pine) were freshly harvested whole branches. The mass of the branches was dominated by needles with comparatively little mass of bark or wood in the twigs. We also tried to control the relative ratio of non-needle to needle mass. In addition, in nearly all

experiments, the needles dominated actual fuel consumption and the branches were minimally burned. However, despite these controls, some variability may have occurred which may impact the emissions [*Coggon et al.*, 2016].

2.2. Experimental Setup

Figure 1 shows a schematic of the experimental setup, which consisted of two identical Teflon smog chambers on the floor of the FSL burn room, with sampling lines connecting them to a shared set of instrumentation located in a mobile laboratory parked immediately outside of the FSL facility. Before each experiment, we flushed both 7 m^3 Teflon smog chambers for at least 12 h with high-efficiency particulate air (HEPA) and activated carbon filtered air. Thirty minutes prior to smog chamber smoke injection, we heated the transfer lines and flushed them with preconditioned air.

We filled the dual smog chambers with emissions using two different procedures: (i) sampling directly out of the FSL exhaust stack ("stack" burn) or (ii) sampling out of the smoke-filled FSL combustion room ("chamber" burn). In the stack burn configuration (7 of 19 dual-chamber experiments), we conducted burns about 2 m below a 1.6 m diameter FSL exhaust stack. The smoke then passed through the FSL exhaust stack, and we sampled the emissions from the top of the stack through an electrically heated (40°C) 15.24 m long, 1.27 cm outer-diameter passivated (Silcosteel-coated; Restek, Bellefonte, PA) stainless-steel transfer line using four ejector dilutors operated in parallel (Dekati, Helsinki, Finland). The mean residence time in the exhaust stack before the sample location was ~5 s; trace-gas measurements indicate that the emissions are well-mixed at this location [*Christian et al.*, 2003]. The ejector dilutors pulled the smoke through the transfer line at a total flow rate of 24.0 L min^{-1} (6 L min^{-1} per dilutor) and injected the smoke into each smog chamber. The ejector diluters operated on dried, HEPA, and activated carbon filtered air preheated to 40°C.

In the chamber burn configuration (12 of 19 dual-chamber experiments), we completely burned the fuel sample and allowed the emissions to fill the 3000 m^3 FSL combustion chamber. After the emissions were well-mixed in the FSL combustion chamber (~20 min after burn completion, as indicated by a suite of gas- and particle-phase instrumentation), we conditioned the chamber injection lines with the smoke for at least 30 min. We then transferred a small portion of the emissions from the FSL combustion chamber into the smog chambers using the four ejector dilutors and 3.048 m long, 1.27 cm outside-diameter heated passivated stainless-steel transfer line heated to 40°C with an inlet placed 3 m above the ground in the middle of the FSL combustion chamber. During the chamber burns, the FSL exhaust stack was retracted into the ceiling.

We injected a controlled, identical quantity of the biomass burning emissions into both smog chambers to achieve ambient plume-like conditions (initial aerosol concentrations ranged from 5–to 90 μg m^{-3}). The initial (preperturbation) aerosol and gas concentrations in each chamber were within 20%. Differences were due to differing volumes of clean air inside of each chamber prior to injection of emissions.

Losses of gases and particles in transfer and sampling lines are always a concern. In both experimental configurations, we heated the passivated stainless steel transfer lines to reduce the loss of semivolatile vapors. However, metal throughout the experimental setup can convert gas-phase species such as hydroperoxides, which are known to form from biomass burning, to more stable products [*Rivera-Rios et al.*, 2014; *Bernhammer et al.*, 2017]. This issue was not investigated in this study. The two experimental configurations also had different length transfer lines (~3.048 m versus ~15.24 m for the chamber and stack burns, respectively). The effect of this difference was also not investigated. *Hennigan et al.* [2011] utilized a very similar sampling setup (~12.192 m sampling line); they measured an aerosol transmission efficiency (using sodium chloride aerosol) of 0.94. No corrections were applied to account for transfer line losses.

2.3. Instrumentation

Gas- and particle-phase instrumentation was located in the Carnegie Mellon University mobile air quality laboratory, located immediately outside the northwestern wall of the FSL combustion chamber. We used an automated three-way valve to control which smog chamber was being sampled by the suite of instruments.

We measured nonrefractory submicron aerosol mass and chemical composition with an Aerodyne High-Resolution Aerosol Mass Spectrometer (HR-AMS), and we measured number size distributions between
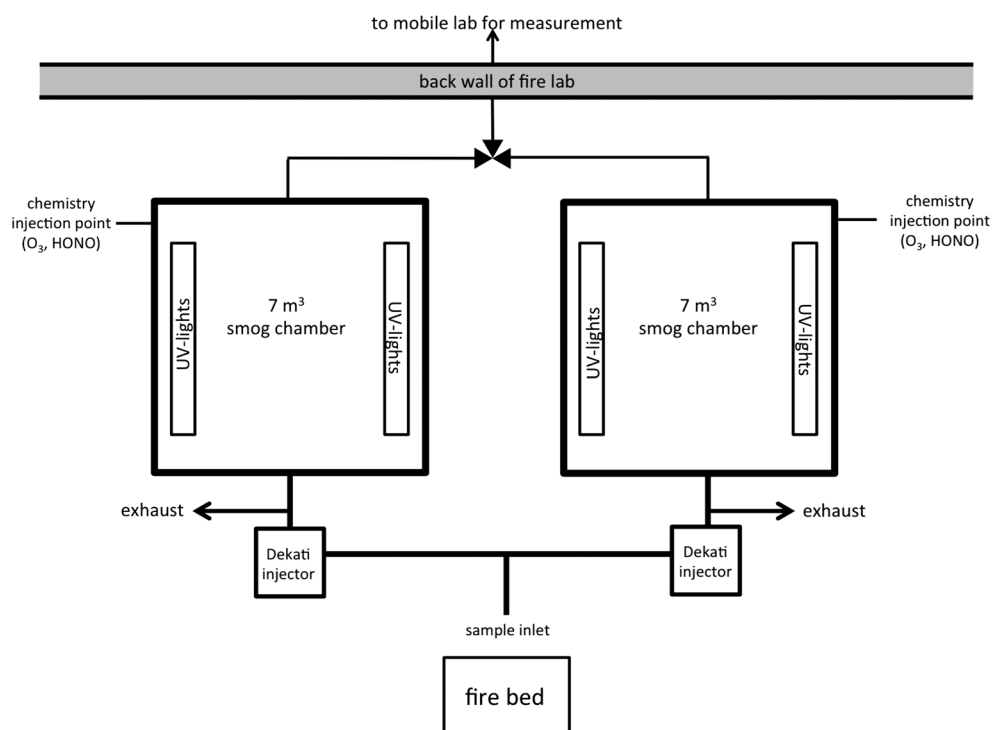
Figure 1. Experimental setup at FLAME-IV.

10.9 and 478 nm with a scanning mobility particle sizer (SMPS, TSI 3936). We converted these SMPS size distributions to volume distributions assuming spherical particles. This assumption is supported by HR-AMS measurements, which indicate that emissions in every experiment were OA-dominated (see section 2.5.1). We measured black carbon (BC) using an aethalometer (Magee Scientific model AE-31) and a single-particle soot-photometer (SP2, N,N-dimethyltryptamine (DMT)). We analyzed the HR-AMS data using the Squirrel and Pika toolkits (http://cires.colorado.edu/jimenezgroup/wiki/index.php/ToFAMS_Analysis_Software).

We monitored concentrations of select volatile organic compounds (VOCs) using a quadrupole and a high-resolution proton-transfer reaction mass spectrometer (PTR-MS, Ionicon, Innsbruck, Austria). We used the measured decay of toluene to infer OH concentrations in the smog chambers for six dual-chamber experiments, which corresponds to 12 individual chamber experiments (OH concentrations are listed in Table S1). In one experiment, both PTR-MS instruments were operating simultaneously, and these measurements yield OH concentrations that were similar within 20%. OH concentrations for each perturbation type were similar within 30% (see supporting information for discussion on estimating OH concentrations). Additional gas-phase measurements included CO_2 (Licor Biosciences Model LI-820), NO_x (Teledyne model 200EU), and O_3 (API model 400A). We calibrated the PTR-MS weekly by measuring a custom blend of gases in nitrogen (Scott-Marrin, Inc., Riverside, California), and we calibrated the other gas-phase monitors daily.

2.4. Experimental Matrix

Table 1 lists all of the dual-chamber perturbation experiments performed at FLAME-IV. As described previously, we used two identical smog chambers to allow simultaneous investigation of two different atmospheric conditions on the same smoke sample. We designed most experiments to isolate the effects of a single perturbation (VOC/NO_x, UV, and dark O_3) on SOA formation. For these single-perturbation experiments, the smoke in the second chamber was aged in the dark with no additional oxidants and therefore served as an unperturbed reference or control. The dark reference chamber also allowed us to evaluate the technique for calculating OA mass enhancement (see section 2.5.1). If we observe no OA mass enhancement in the dark, unperturbed chamber, then we are confident that the changes in the OA mass enhancement in the perturbed chamber were due to the perturbation and not some other effect. In some

Table 1. List of Dual Smog Chamber Perturbation Experiments Conducted During FLAME-IV[a]

			Number of Experiments		
Purpose	Perturbation Chamber	Reference Chamber	PP	BS	Other
Effects of UV	UV	Dark	2	2	2
Effects of dark O_3	O_3	Dark	1	1	–
Effects of VOC/NO_x	HONO + UV	UV	2	2	–
Dark O_3 versus UV	O_3	UV	1	1	4
Chamber precision	UV	UV	–	1	–
Total			6	7	6

[a]Multiple experiments were conducted using ponderosa pine (PP) and black spruce (BS). A full list of experiments and fuels used can be found in the supporting information.

experiments, we perturbed the smoke in both chambers simultaneously. For example, the "dark O_3 versus UV" experiments compare the effects of UV light initiated photo-oxidation to dark O_3 exposure. Finally, we conducted one "chamber precision" experiment to investigate if smoke in each chamber behaved similarly when perturbed in the exact same way.

In all experiments, we initiated perturbations 15–45 min after filling both smog chambers. We used the preperturbation period to characterize the primary gas and particle concentrations. An additional advantage of the dual-chamber design is that if we did not perturb the reference chamber, we could initiate the perturbation chemistry quickly after filling, thus reducing the effects of wall losses and other chamber artifacts compared to a single-chamber experiment where postfilling characterization is essential.

We designed the "effects of UV" experiments to study the effects of photo-oxidation, the light-initiated chemistry that includes the formation OH and O_3 on SOA formation. In these experiments, we initiated photo-oxidation by turning on UV lights (GE model 10526 blacklights) in one chamber while leaving the other dark as a reference. UV irradiation of biomass burning emissions in these experiments produced OH radical concentrations of ~1×10^6 molecules cm^{-3} (see supporting information), which was inferred from the measured decay of toluene. Modest levels of ozone (30–50 ppbv) were formed in the UV-only experiments.

We designed the "effects of dark O_3" experiment to investigate the effects of dark ozonolysis on SOA formation. We injected ozone (500–1000 ppbv) into one chamber using an ozone generator (Azco Industries Ltd. model HTU-500, Langley, British Columbia), while not perturbing the other chamber (which therefore served as a reference). Both chambers were dark. There was always substantial ozone left in the dark + O_3 chamber at the end of these experiments, indicating that the experiments were not oxidant limited. Ozone reacts with unsaturated organics, including known SOA precursors such as α-pinene. The amount of unsaturated organics in biomass plumes is often not known. However, elevated (up to ~100 ppb) ozone levels have been observed in biomass burning plumes [*Andreae*, 1990; *Akagi et al.*, 2013]. Ozonolysis of unsaturated emissions (e.g., alkenes and monoterpenes) can also produce significant amounts of OH and thus oxidize other constituents, including saturated SOA precursors such as large alkanes [*Paulson and Orlando*, 1996]. Recent work by *Bruns et al.* [2016] has shown that aromatics, which react much more rapidly with OH than O_3, may play an important role in SOA formation from biomass burning emissions. During dark ozonolysis experiments, OH concentrations were ~2×10^5 molecules cm^{-3}, based on the measured decay of toluene (see supporting information). This is an order of magnitude lower than OH levels in our photo-oxidation experiments.

We designed the "effects of VOC/NO_x" perturbation to study the effects of photo-oxidation in different NO_x regimes, which can have complex effects on SOA formation [*Kroll and Seinfeld*, 2008; *Hennigan et al.*, 2011; *Chuang and Donahue*, 2016]. NO_x (specifically NO) affects the fate of peroxy radicals. The RO_2 + HO_2 (high VOC/NO_x) pathway generally produces lower volatility products than the RO_2 + NO (low VOC/NO_x) pathway. However, the effects of VOC/NO_x on SOA formation vary by precursor, making it difficult to predict the net effect of changing VOC/NO_x on highly complex precursor mixtures such as biomass burning emissions. For example, photo-oxidation of small hydrocarbons (<C_{10}) under low VOC/NO_x conditions (RO_2 + NO pathway) lowers SOA production [*Hurley et al.*, 2001; *Song et al.*, 2005; *Ng et al.*, 2007; *Zhang et al.*, 2007; *Chan et al.*, 2009] versus increasing SOA production for larger (>C_{12}) hydrocarbons [*Lim and Ziemann*, 2005].

In the "effects of VOC/NO$_x$" experiments, both chambers were exposed to UV lights, but nitrous acid (HONO) was added to one of the smog chambers following the method of *Ng et al.* [2007]. In this experiment, the UV-only chamber served as the reference. Before photo-oxidation, the NO levels in the both chambers were low (a few to ~30 ppbv of NO; Table S4). Irradiation of HONO produces both OH and NO. The additional NO lowered VOC/NO$_x$ ratio in the UV + HONO chamber relative to the UV-only chamber. NO also reacts rapidly with ozone. Ozone concentrations were always below detection limit (a few ppbv) in the UV + HONO chamber versus the production of 30–50 ppbv of ozone in the UV-only chamber. The UV + HONO chamber had higher OH concentration (~2×10^6 molecules cm^{-3}, see supporting information), about twice the OH concentration in the UV-only chamber.

We designed the "dark O$_3$ versus UV" experiments to compare daytime versus nighttime oxidation (photo-oxidation versus dark ozonolysis). In these experiments, we perturbed one chamber with UV light while perturbing the other by adding in excess of 500 ppb of O$_3$ in the dark. Although dark ozonolysis forms OH, the amount of OH in chambers with ozone (inferred from the decay of toluene measured by the PTR-MS) was ~2×10^5 cm^{-3}, nearly an order of magnitude lower than OH levels in the chamber exposed to UV light.

2.5. Data Analysis

2.5.1. OA Mass Enhancement

We derived the OA mass enhancement following the methodology of *Grieshop et al.* [2009] and *Hennigan et al.* [2011] using the OA-to-BC ratio to account for the loss of particles and vapors to the chamber walls. The organic aerosol mass enhancement ratio is

$$\text{OA mass enhancement} = \frac{OA_t/BC_t}{OA_0/BC_0} \tag{1}$$

where OA$_t$ and BC$_t$ are the OA and BC concentrations at time t after the onset of the perturbation, respectively, and OA$_0$ and BC$_0$ are the OA and BC concentrations just before the perturbation is initiated. This corrects for loss of particle mass to the chamber walls and assumes that the vapors remain in equilibrium with the particles lost to the chamber walls ($\omega = 1$) [*Weitkamp et al.*, 2007]. Black carbon (BC) mass concentrations were measured using a single-particle soot-photometer (SP2, DMT) or an aethalometer (Magee Scientific model AE-31) when SP2 measurements were unavailable. These instruments use fundamentally different principles. To evaluate quantify potential biases caused by SOA formation and optical measurement of BC using an aethalometer (e.g., due to changes in the mass absorption cross section due to formation of brown carbon [*Saleh et al.*, 2013] or lensing), we operated both BC instruments in nine dual-chamber experiments. In these experiments, the OA mass enhancements derived using measurements from both BC instruments were within 25% of each other with no bias (Figure S2 in the supporting information).

We estimated the OA mass concentration from the particle volume calculated from the SMPS measurements; we did not use the HR-AMS to calculate OA mass enhancements due to uncertain changes in the HR-AMS collection efficiency over the course of each experiment. The particle volume was calculated, assuming spherical particles. This was a good assumption because BC mass concentrations were much lower than SMPS-derived mass concentrations (<5% SMPS mass), and HR-AMS measurements indicate that organics dominated (>90%) nonrefractory PM mass before and after the perturbations. The BC/OA ratios observed in these experiments (0.01–0.05) are similar to field measurements of biomass burning plumes [*Jolleys et al.*, 2015].

To convert the SMPS measured volume to particle mass requires knowing the POA and SOA density. In 11 of 19 experiments, we calculated particle density by comparing the aerosol volume size distributions (determined by the SMPS) and aerosol mass size distributions (determined by the HR-AMS), following the method described by *Bahreini et al.* [2005]. The average initial ($t = 0$) particle density was 1.42 ± 0.13 g cm^{-3}, and the average final ($t = 2$ h) particle density following perturbation was 1.55 ± 0.22 g cm^{-3}, indicating an average density change of +8.8% in perturbation chambers. In 8 of 19 experiments, particle signal was too low to produce reliable volume and mass distributions (i.e., low signal-to-noise data) to determine particle density. For these experiments, we used the average initial and final particle density calculated for the other experiments. The particle density in the dark (no perturbation) chambers remained essentially constant (average density change of +0.5%).

2.5.2. Dual-Chamber Enhancements

A second metric used to describe SOA formation, the dual-chamber enhancement (DUCE), quantifies the relative changes in OA mass between the two chambers:

$$\text{DUCE} = \frac{\text{OA mass enhancement}_{\text{perturb}}}{\text{OA mass enhancement}_{\text{reference}}} \qquad (2)$$

where OA mass enhancement$_{\text{perturb}}$ is the OA mass enhancement (equation (1)) in the perturbed chamber and OA mass enhancement$_{\text{reference}}$ is the OA mass enhancement in the reference chamber.

The DUCE metric quantifies the effect of a perturbation (UV irradiation, NO$_x$, and ozone) on OA mass enhancement relative to a reference condition for smoke from the same fire. Therefore, the DUCE metric isolates the effects of different perturbations by controlling for smoke composition; therefore, any difference in OA mass enhancements between the two chambers can be attributed to the perturbation and not to differences in emissions. A DUCE >1 indicates that the perturbation caused a higher OA mass enhancement (or lower mass loss) compared to the reference chamber, and a DUCE <1 indicates that the perturbation caused a lower OA mass enhancement (or a higher loss) compared to the reference. A limitation is that the DUCE only quantifies the relative, not absolute, change in OA mass.

3. Results and Discussion

In this section, we first present time series of key data from a typical experiment to illustrate the calculation of OA mass enhancement ratios and the DUCE metric. We then compare OA mass enhancement ratios from all experiments and briefly discuss the chemical evolution of OA mass spectrum. Finally, we use the DUCE metric to isolate the effects of different perturbations on emissions from the same fire.

3.1. OA Mass Enhancements

To illustrate data from a typical experiment, Figures 2a and 2b show time sequences of particle mass concentrations inferred from the SMPS data and SP2-measured BC mass concentrations during an "effects of VOC/NO$_x$" perturbation experiment with black spruce (burn 126). At $t = 0$, we perturbed one chamber with UV + HONO (Figure 2a), while exposing the reference chamber to UV only (Figure 2b). After the perturbation, the PM mass concentrations in the "HONO + UV" chamber (Figure 2a) continued to decrease, while the PM mass concentrations in the "UV-only" chamber (Figure 2b) increased and then decayed at a slower rate, indicating substantial SOA formation (in excess of wall loss).

Figure 2c shows the evolution of the OA mass enhancement ratios for the black spruce experiment calculated from the data shown in Figures 2a and 2b. The OA mass enhancement ratio of the "HONO + UV" chamber (blue triangles) increased to around 1.6 (indicating modest production of new OA mass), while the OA mass enhancement ratio of the "UV-only" reference chamber increased to 3.5, indicating that SOA formation more than tripled the wall-loss-corrected OA mass. In Figure 2d, the time series of DUCE values compare the OA mass enhancement between the two chambers. DUCE values at the end of the experiment were ~0.5, indicating that OA mass enhancement in the HONO + UV chamber was about 50% less than that in the UV-only chamber.

OA mass enhancements measured 2 h after the perturbation for each of the 19 dual-chamber experiments performed at FLAME-IV are shown in Figure 3. This corresponds to 38 individual chamber experiments of which 30 were perturbation experiments (UV light, UV + HONO, or dark O$_3$) with the balance (8) being dark reference. OA mass enhancement ratios ranged from 0.7 to 4.4. The largest OA enhancement (4.4) was observed in a UV-only black spruce experiment. The smallest (0.7, indicating a 30% loss in OA) was smoke from burning ocote in a "rocket" cook stove.

We performed one "chamber precision" experiment (burn 51) by subjecting black spruce emissions in each smog chamber to the same perturbation (UV irradiation). For this experiment, the emissions in each chamber responded similarly with OA mass enhancements of 4.4 and 4.2, indicating essentially the same SOA production when the smoke was subjected to the same emissions and conditions. This experiment suggests that the dual-chamber approach has reasonable precision.
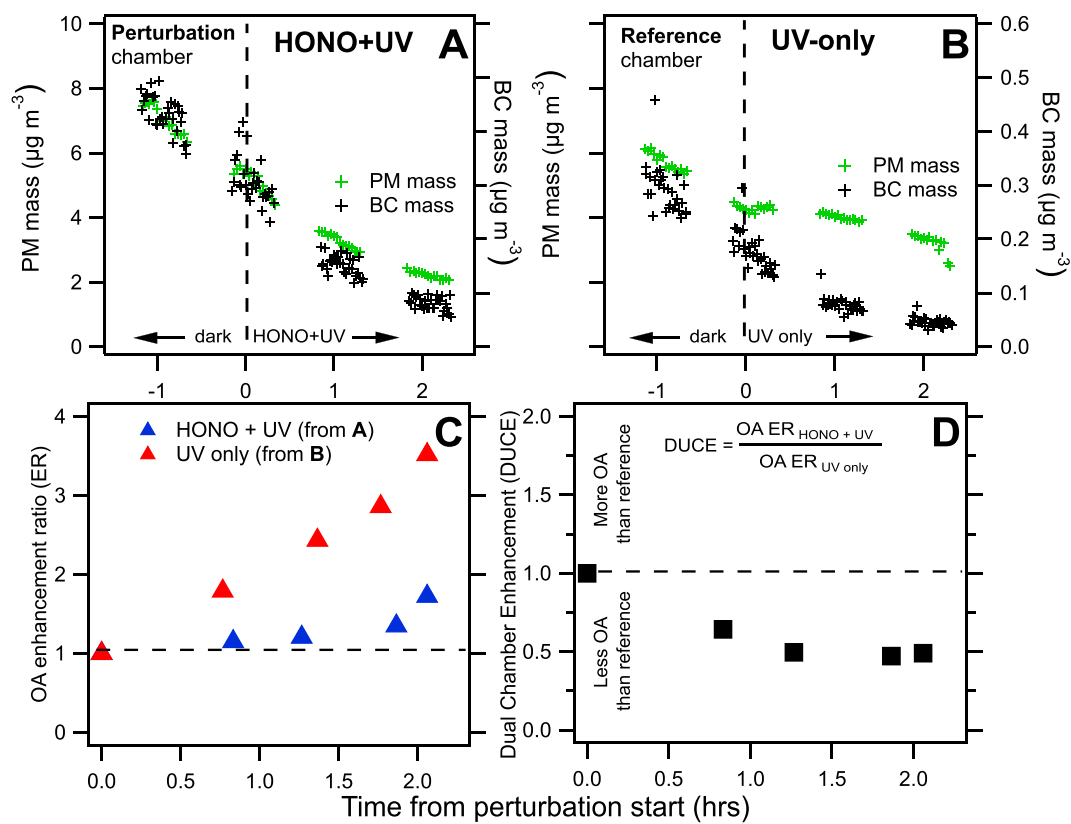
Figure 2. Time series of measured PM and BC mass concentrations for "effects of VOC/NO$_x$" experiment. (a) HONO + UV chamber; (b) UV-only chamber; (c) OA mass enhancement ratios for both chambers; and (d) DUCE values using the UV-only chamber as reference.

We performed multiple experiments with two biomass types (black spruce and ponderosa pine). Perturbing the smoke from these fuels almost always generated some SOA (OA mass enhancements greater than or equal to 1). The average OA mass enhancements for perturbation experiments with black spruce and ponderosa pine were 2.1 ± 1.3 and 1.6 ± 0.5, respectively. However, Figure 3 indicates there was substantial burn-to-burn variability in OA enhancement with these fuels. For example, OA enhancements for black spruce smoke ranged from 1 (no enhancement) to 4.4 across seven separate UV-only experiments. Similar variability was observed for ponderosa pine with OA enhancement ratios ranging from 1 to 2.5 across five UV-only experiments. For each of these experiments the same fuel was burned under nominally the same conditions. This suggests that fuel type may not be a good indicator of SOA production.

Hennigan et al. [2011] performed similar chamber experiments with ponderosa pine and black spruce smoke as part of the FLAME-III experiments. For ponderosa pine, *Hennigan et al.* [2011] measured substantially less OA enhancement than we measured here: 0.9 ± 0.1 versus 1.6 ± 0.7 for UV-only experiments. For black spruce, *Hennigan et al.* [2011] measured similar OA mass enhancements (2.9 ± 1.0) as this study (2.4 ± 1.5).

Because fuel type does not appear to be a robust indicator of SOA production, Figure 4 combines data from experiments with different fuels to focus on the effects of different perturbations. Figure 4a compares cumulative distributions of the OA enhancement for the dark and perturbation experiments. In the vast majority of the experiments with a perturbation (UV, UV + HONO, or dark O$_3$) there was some enhancement of OA mass (OA mass enhancement > 1). The median (50th percentile) OA mass enhancements were 1.0 for dark, unperturbed chambers (no OA mass enhancement) and 1.5 for perturbed chambers (a 49% growth in OA mass). Therefore, simply aging emissions in the dark without oxidants did not produce SOA. Although perturbed chamber OA mass enhancements were as high as 4.5, the 75th percentile OA mass enhancement for the perturbation experiments is 2. This means that 25% of the perturbation experiments FLAME-IV (n = 30) at
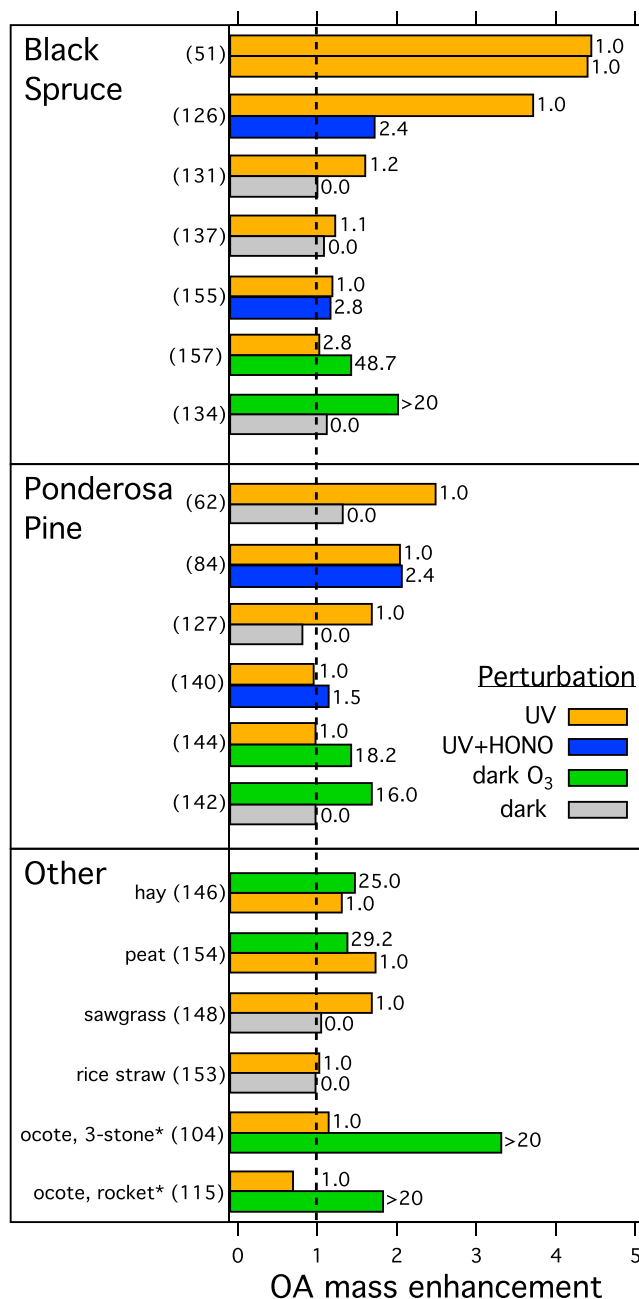
Figure 3. End of experiment OA mass enhancements measured at FLAME-IV. Each dual-chamber experiment is labeled with its burn number in parentheses. Numbers to the right of the bars indicate the estimated equivalent atmospheric oxidation time, in hours. These estimated times assume average plume [OH] of 2×10^6 molecules cm^{-3} and [O$_3$] of 60 ppb [*Parrington et al.*, 2013].

least doubled OA mass. In comparison, only 10% (3 out of 30) showed a decrease in OA mass and only 1 showed a substantial (30%) decrease.

In Figure 4b box-and-whisker plots compare the OA mass enhancement ratios for different perturbations (grouping the data for different biomass types). These ratios correspond to 2 h of photo-oxidation ($t = 2$ h). UV-only perturbations resulted in the largest average OA mass enhancements of 1.8 ± 1.1 (OA mass, on average, increased by 81%). However, the large standard deviation reflects substantial experiment-to-experiment variation; the UV-only experiments included both the top three and the lowest six enhancements, including the one experiment with a clear loss in OA mass. Dark ozonolysis also created substantial OA mass enhancement. Perturbations of >500 ppb of ozone created an average OA mass enhancement of 1.8 ± 0.6. UV + HONO perturbations caused an OA mass enhancement of 1.5 ± 0.5. "Blank" experiments in which ozone was injected into a clean chamber without biomass smoke emissions formed no OA.

OA mass enhancements measured during FLAME-III [*Hennigan et al.*, 2011] fall within the 25th and 75th percentiles of the new data. FLAME-III only used UV and UV + HONO perturbations (third and fourth columns in Figure 4b). We extend the results of *Hennigan et al.* [2011] by showing that dark ozonolysis creates OA mass enhancements. The dual-chamber method also confirms that the OA enhancements are not artifacts of burn-to-burn fluctuations during nominally identical experiments.

3.2. Chemical Evolution of BBOA

Figure 5 shows select OA mass fragments measured with the HR-AMS for the same "effects of VOC/NO$_x$" experiment presented in Figure 2. The organic fraction of m/z 44 (CO$_2^+$ peak) increased in both chambers after perturbation ($t = 0$), but it increased significantly more in the UV-only chamber compared to the UV + HONO chamber. This mirrors the difference in OA mass enhancement ratios shown in Figure 2. m/z 44 is a fragment of organic acids that is a marker ion for oxidized organic aerosol (OOA). The organic
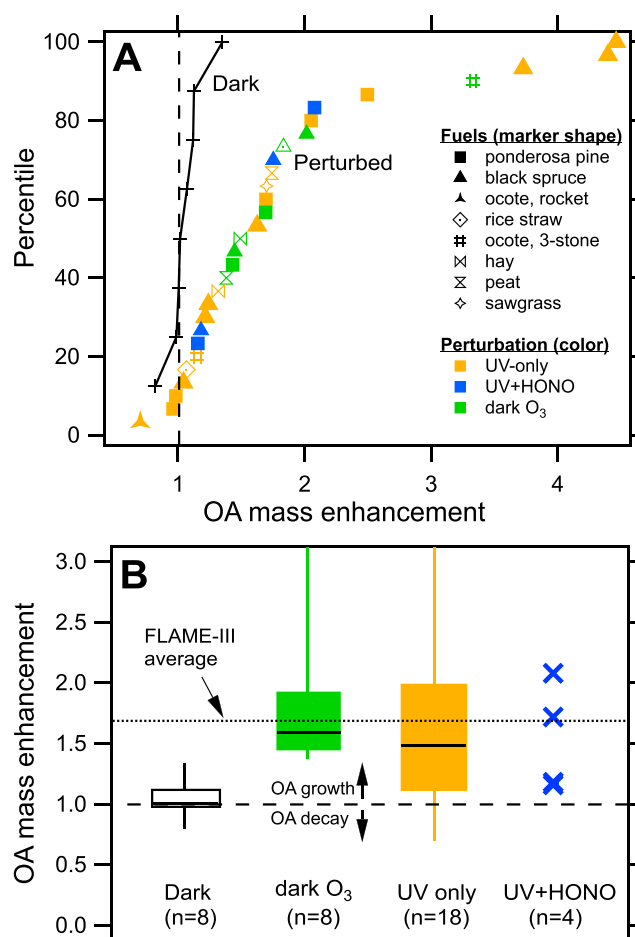
Figure 4. (a) Cumulative distribution of OA mass enhancements calculated for dark, unperturbed (black trace) and perturbed (colored markers) chambers after 2 h of oxidation. (b) Box-and-whisker plots of OA mass enhancement ratios group by perturbation from all chamber experiments conducted at FLAME-IV. The boxes indicate the 25th and 75th percentiles with the interior line indicating the median value. The whiskers indicate min and max values. The average OA mass enhancement reported from FLAME-III is shown as a dotted line [*Hennigan et al.*, 2011].

fraction of *m/z* 60 fragment is often used as a tracer for fresh biomass burning emissions. It is associated with levoglucosan ($C_6H_{10}O_5$), which is formed from the pyrolysis of cellulose and a common tracer for biomass burning emissions [*Simoneit et al.*, 1999]. The *m/z* 60 fragment decreased in both chambers (see supporting information), reflecting the production of SOA. These changes in the HR-AMS mass spectra are consistent with laboratory data from *Hennigan et al.* [2011] and field studies, e.g., *Hawkins and Russell* [2010].

AMS measurements indicate that unperturbed emissions contained organic nitrates, but perturbations caused the formation of inorganic nitrates. The nitrate group from organic nitrates typically produces much higher NO^+/NO_2^+ ion ratios (*m/z* 30:46) than ammonium nitrate [*Farmer et al.*, 2010]. For the unperturbed emissions, the ratio of NO^+/NO_2^+ ranged from 3.6 to 12.6, indicative of organic nitrates (ammonium nitrate fragments in our AMS have an NO^+/NO_2^+ ion ratio of ~0.3). Perturbations reduced the NO^+/NO_2^+ ratio throughout the experiment, suggesting formation of ammonium nitrate, which decreased the contribution from organic nitrates.

Figure 6 summarizes changes in OA chemical composition across the set of experiments. It presents box whisker of oxygen-to-carbon (O/C) ratio and the organic fraction of *m/z* 60 (f_{60}) separated into no perturbation and perturbation experiments. There were essentially no changes in OA O/C ratios in dark, unperturbed experiments (average O/C = 0.21 ± 0.04), but every perturbed experiment showed significant increases in the O/C ratio (median increase of 67% over initial O/C; average postperturbation O/C = 0.34 ± 0.09), consistent with perturbations causing substantial oxidation. The fraction of *m/z* 60 decreased in nearly all perturbation experiments. Figure 5 indicates that even when there was no OA mass enhancement (i.e., Figure 2b), perturbations caused the chemical composition of the OA mass to become oxidized. *Hennigan et al.* [2011] reported the same behavior with photo-oxidized biomass burning emissions from FLAME-III. Increased oxidation without OA production has also been observed in field studies [*Hawkins and Russell*, 2010; *Jolleys et al.*, 2012]. Additional analysis of the HR-AMS data and SOA mass closure from FLAME-IV will be the focus of an upcoming study.

3.3. Effects of Atmospheric Perturbations on OA Mass Enhancements

Although the OA mass enhancement ratio quantifies the production (or loss) of OA during an experiment, the dual-chamber approach isolates the effects of different atmospheric perturbations on SOA formation relative to a reference condition by using emissions from the same burn. In Figure 7 we present box-and-whisker
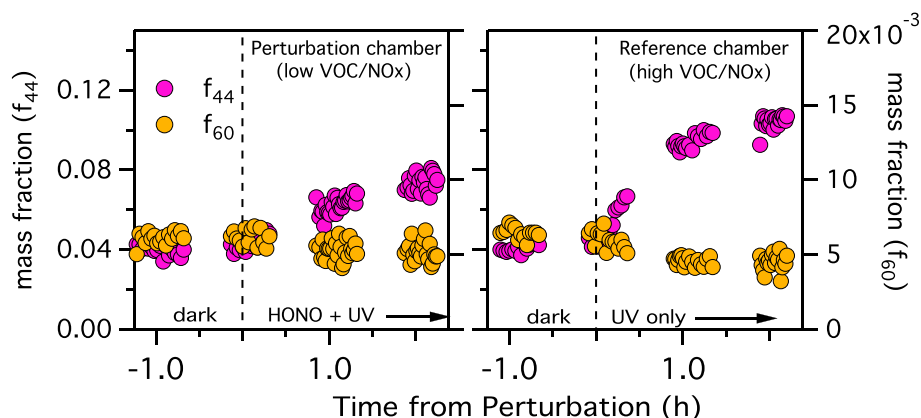
Figure 5. HR-AMS mass fraction time series for the perturbation and reference chambers during an "effects of VOC/NO$_x$" experiment (burn #126). f_{44} indicates the organic fraction of m/z 44 (CO$_2^+$), a fragment of organic acids that is a major marker ion for oxidized organic aerosol (OOA) by AMS analysis. f_{60} is the organic fraction of m/z 60, a mass fragment commonly associated with levoglucosan (C$_6$H$_{10}$O$_5$).

plots for dual-chamber enhancement (DUCE) values, calculated for each set of paired dual-chamber perturbation/reference experiments using equation (2). All DUCE values correspond to conditions at t = 2 h.

We performed one "chamber precision" experiment by subjecting the emissions in each smog chamber to the same perturbation (UV irradiation). The emissions from each chamber responded similarly when perturbed in the same manner with OA mass enhancements of 4.4 and 4.2. This corresponds to a DUCE of 1.05 (a DUCE of 1 indicates that both chambers have the same OA mass enhancement ratio).

The first box-and-whisker in Figure 7 represents the distribution of DUCE values for the UV-only/unperturbed-dark paired experiments. The median DUCE for this perturbation is 1.5, which means that on average, a chamber perturbed with UV irradiation produced ~53% more OA mass than a dark, unperturbed chamber filled with the same smoke. This is essentially the same as the average OA enhancement ratio shown for the UV-only experiments in Figure 3b because there was no OA mass enhancement in the dark control chamber used as the reference. By definition, if there is no change in the reference, then the DUCE value is the same
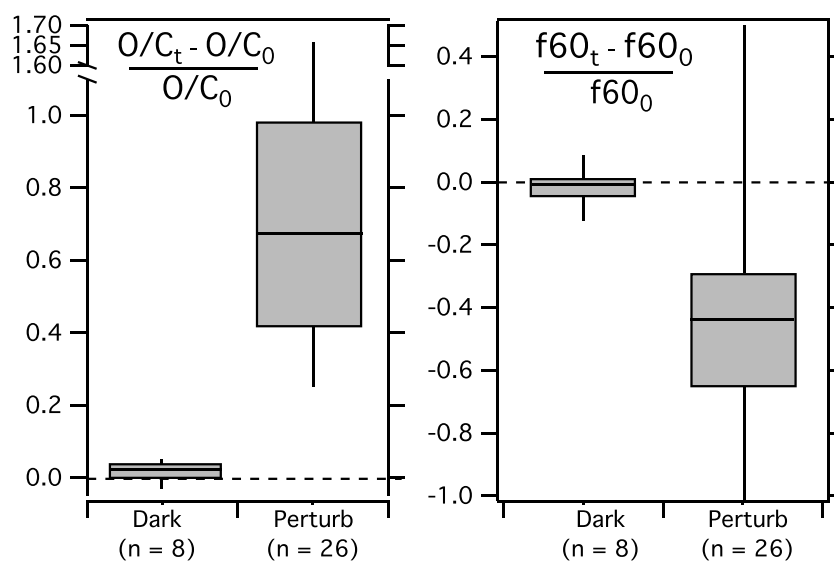

Figure 6. Changes in OA chemical composition in response to perturbation (i.e., UV-only, UV + HONO, and dark O$_3$) and in dark, unperturbed chamber. O/C is the oxygen-to-carbon ratio, derived from HR-AMS analysis. f_{60} is the organic mass fraction of m/z 60, a mass fragment associated with levoglucosan (C$_6$H$_{10}$O$_5$). The boxes indicate the 25th and 75th percentiles with the interior line indicating the median value. The whiskers indicate min and max values.

Figure 7. Box-and-whisker plots of DUCE values from all chamber experiments conducted at FLAME-IV. The x axis labels indicate the "perturbation" conditions (numerator) and the "reference" conditions (denominator). The boxes indicate the 25th and 75th percentiles with the interior line indicating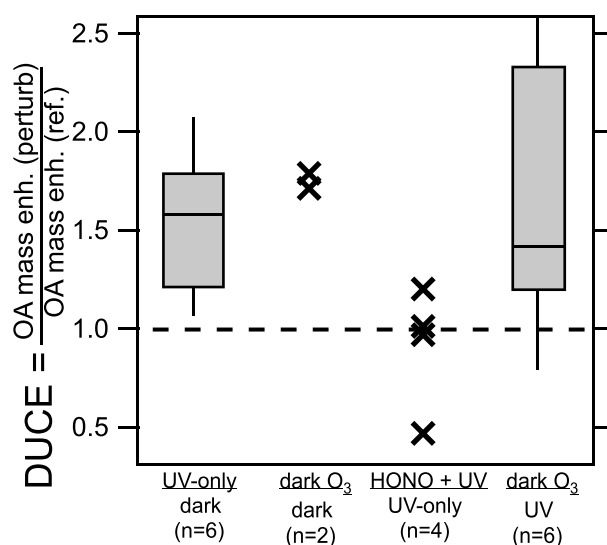 the median value. The whiskers indicate min and max values. Only symbols are shown for dark O_3 and HONO + UV pertubations given the limited number of experiments.

OA enhancement ratio in the perturbed chamber. As expected given the variability in the UV-only OA enhancement ratios, there is significant variability in the UV-only DUCE values. This was driven by variability of the results in the perturbed chamber (the dark unperturbed chamber always produced no OA; Figure 4).

DUCE values for dark O_3 versus unperturbed-dark are shown in the second column of Figure 7. The average dark O_3 DUCE value is 1.75, indicating that on average, a chamber dark ozonolysis produced ~75% more OA mass than a dark, unperturbed chamber filled with the same smoke. Again, this is essentially the same value as the OA mass enhancement for the dark O_3 experiments because there was no OA mass enhancement in the dark chamber experiments.

Since there were no changes in the dark (unperturbed) control chamber, the DUCE values provide more insight into the results from experiments when both chambers are perturbed (e.g., dark O_3 versus UV-only and HONO + UV versus UV-only). The average DUCE of dark O_3 versus UV-only paired experiments (the last symbol in Figure 7) was +1.7 ± 0.7, which means that on average, there was 72% more OA production in the dark O_3 chamber than in the UV-only chamber. This could be interpreted that ozone is a more important oxidant for forming SOA in biomass smoke than OH. However, the ozone levels used here are much higher than those reported in ambient biomass burning plumes (>500 ppb versus 50–100 ppb O_3, respectively [*Parrington et al.*, 2013]). In contrast the OH levels in UV-only chamber were modest, ~1.0×10^6 molecules cm^{-3} (see supporting information). This is lower than typical ambient plumes, which have OH concentrations that range between 5×10^6 and 1×10^7 molecules cm^{-3} [*Yokelson et al.*, 2009; *Akagi et al.*, 2012]. Therefore, the atmospheric equivalent oxidant exposure in the dark O_3 chamber was 5 to 10 times higher than the OH exposure in the UV-only chamber. Consequently, the greater OA enhancement in the dark O_3 chamber may be simply due to the much higher oxidant exposures compared to the UV-only chamber.

Previous chamber experiments suggest that SOA formation in dilute biomass smoke may depend on the VOC/NO$_x$ ratio, with lower production under high NO$_x$ conditions [*Grieshop et al.*, 2009; *Hennigan et al.*, 2011]. The OA enhancement ratios in Figure 4 are consistent with that hypothesis; on average, there was slightly less SOA production in the UV + HONO chamber than in the UV-only chamber (OA mass enhancements of 1.5 ± 0.5 versus 1.8 ± 1.1, respectively) despite higher OH concentrations in HONO chamber. However, the difference is not statistically significant. In addition, our UV-only experiments were not always paired with a UV + HONO chamber, which means that a comparison of OA enhancement ratios does not control for smoke composition. Controlling for smoke composition is especially important, given the large burn-to-burn variability in OA mass enhancement ratios for different experiments performed with the same fuel burned under nominally the same conditions (e.g., Figure 4). Previous laboratory studies of NO$_x$ effects on biomass smoke did not control for burn-to-burn variability (*Grieshop et al.* [2009] or *Hennigan et al.* [2011]).

The DUCE values in Figure 7 control for burn-to-burn variability to isolate the effects of NO$_x$ on the same smoke. Figure 7 shows that the average DUCE value for four paired "effects of VOC/NO$_x$" experiments was 0.9 ± 0.3. This indicates that on average, similar amounts of SOA were formed when the same smoke was perturbed simultaneously in the UV-only and UV + HONO chambers. However, one cannot conclude that
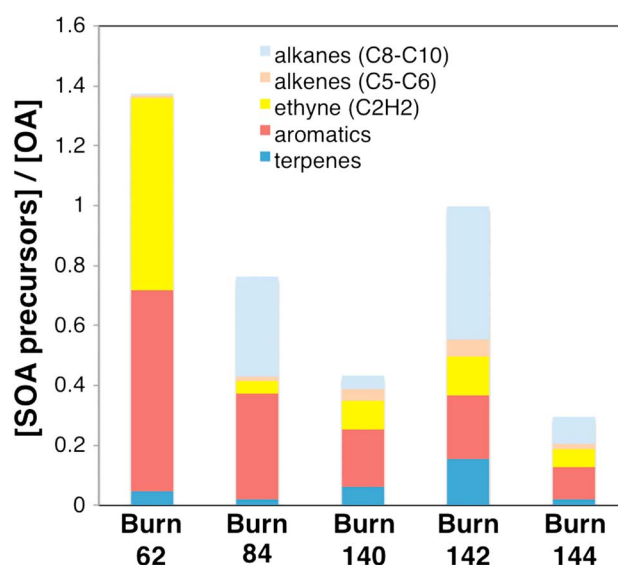
Figure 8. Ratio of initial concentration of select classes of SOA precursors to initial OA concentration. Data are from five different ponderosa pine experiments.

there are no effects of NO_x, given the complexity of the experiments. For example, PTR-MS measurements indicate that the average OH exposure in the UV + HONO chamber was nearly 2 times that in the UV-only chamber (2×10^{10} molecules cm^{-3} s versus 6×10^9 molecules cm^{-3} s, respectively). Therefore, the additional OH oxidation in the UV + HONO (high-NO_x) chamber did not, on average, cause additional SOA production. However, another effect of the HONO addition was to change O_3 concentrations; the UV + HONO chamber had essentially no ozone versus 30–50 ppbv of ozone were produced in the UV-only chamber. These differences in oxidant concentrations make it difficult to draw robust conclusions about any NO_x effects, specifically whether the effects of NO_x are to just change oxidant levels or if it also influences the SOA yield of biomass smoke due to changes in peroxy radical branching.

Figure 7 also indicates that the DUCE values for the "effects of VOC/NO_x" experiments were highly variable, ranging from 0.5 (lower OA mass enhancement in UV + HONO versus UV-only chamber) to 1.2 (higher OA mass enhancement in UV + HONO versus UV-only chamber). DUCE values were variable despite using the same smoke for each paired perturbation experiment. This suggests that the differences in OA mass enhancement ratios between the UV + HONO and UV-only experiments shown in Figure 4 are likely due factors other than VOC/NO_x, most likely differences in smoke composition. For example, SOA production from aromatics is much more sensitive to NO_x than SOA production from large alkanes [*Hurley et al.*, 2001; *Song et al.*, 2005; *Ng et al.*, 2007; *Zhang et al.*, 2007; *Chan et al.*, 2009]. Unfortunately, we do not have sufficient organic composition data to isolate these sorts of effects.

The large variability in both the OA mass enhancement ratios (Figure 3) and DUCE values (Figure 7) suggests that the atmospheric perturbations studied here are not the dominant factor controlling the SOA formation. The variability is likely largely due to variation in the underlying composition of the emissions. To illustrate this variability Figure 8 shows SOA precursor emissions from five ponderosa pine experiments. The precursors were measured using whole air samples collected using 2 L stainless steel canisters that were analyzed using a gas chromatography equipped with flame-ionization and mass-selective detectors to quantify concentrations of 49 volatile organic compounds (VOCs)—C2 to C10 hydrocarbons, including alkanes, alkenes, and single-ring aromatics [*Simpson et al.*, 2001]. SOA precursors were defined as C8–C10 alkanes (alkanes larger than C10 were not quantified), C5–C6 alkenes (alkenes larger than C6 were not quantified), acetylene [*Volkamer et al.*, 2009], single-ring aromatics (benzene, toluene, ethylbenzene, and m/p/o-xylene and styrene), and monoterpenes (isoprene, α-pinene, and β-pinene).

Figure 8 underscores that the mix of SOA precursor emissions is highly variable. Because OA mass enhancement, by definition, describes the change of OA mass relative to the initial OA concentration, Figure 8 shows initial SOA precursor concentrations for each burn normalized by the initial OA concentration measured in the chamber immediately after filling. Despite the same nominal experimental conditions, there is substantial variability in the ratio of SOA-precursor-to-OA-mass emissions across this set of ponderosa pine experiments.

Recently, *Bruns et al.* [2016] suggested that aromatic compounds may contribute the bulk of SOA production for biomass burning emissions. We found no correlation between initial concentrations of aromatics and end-of-experiment OA mass enhancement (see Figure S3). The substantial SOA production in the dark ozone experiments also suggests that precursors other than aromatics are important. Additionally, we found no
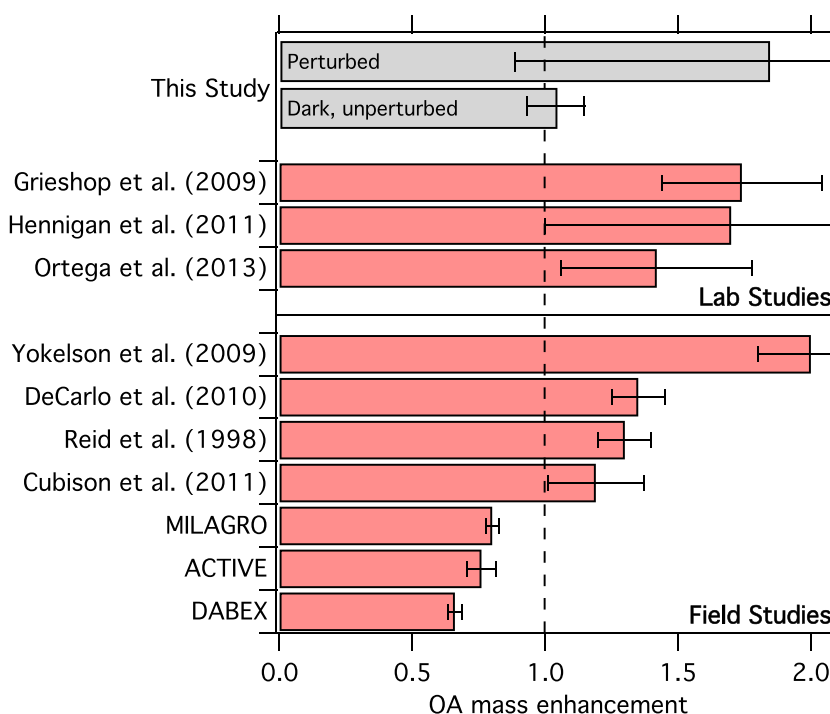
Figure 9. Comparison of this study versus select past studies. The error bars represent standard deviation. MILAGRO, ACTIVE, and DABEX were field studies reported in *Jolleys et al.* [2012].

correlation between the modified combustion efficiency (values in the supporting information) and the amount or fraction of any particular gas-phase constituent in the emissions. It does not appear possible to link precursor emissions to the burn properties that we measured.

4. Conclusions and Atmospheric Implications

Our experiments indicate that photo-oxidation and dark ozonolysis can drive SOA formation in biomass burning emissions. Figure 9 compares our new OA mass enhancement ratios to data from selected published lab and field studies. The published data in Figure 9 are not exhaustive but include a range of prior laboratory and field data sets.

Our OA mass enhancements fall well within the range of published laboratory studies. However, Figure 9 shows that OA mass enhancement ratios reported in laboratory studies are typically higher than those reported from field studies. One reason may be that chamber experiments are typically performed at a fixed dilution ratio, whereas real plumes are continuously diluted, which alters the gas-to-particle partitioning of semivolatile OA [*Grieshop et al.*, 2009]. In the current study, most perturbations increased wall-loss corrected OA concentrations, shifting the gas-particle partitioning toward the particle phase as the experiment progressed. In real plumes, OA concentrations decrease (even if there is SOA production) as the plume is transported away from the source due to dilution. This dilution causes evaporation of semivolatile constituents, reducing the OA mass enhancement compared to no dilution [*Grieshop et al.*, 2009]. We can estimate the magnitude of this effect using the volatility distribution of biomass burning OA from 2013. For example, diluting primary combustion emissions from an OA concentration of 25 $\mu g\,m^{-3}$ (representative for this study) by a factor of 4 causes ~20% loss of OA mass due to evaporation. Therefore, dilution-driven evaporation will cause OA mass enhancement ratios derived from atmospheric data to be systematically lower than those measured in smog chambers without dilution.

Similar to previous field and laboratory studies, our results highlight that large variability is a consistent feature of SOA formation in biomass burning smoke. By performing dual-chamber experiments, we isolated the effects of different atmospheric perturbations on the same smoke. One goal was to quantify the contribution

of different perturbations to the variability in SOA formation. Our results suggest that the large variability in SOA formation is much more influenced by burn-to-burn variability of emissions than differences in atmospheric perturbations. For example, we found no consistent trends in the effects photo-oxidation in high- versus low-NO_x conditions on SOA formation. The underlying cause appears to be that burns of the same fuel under nominally the same conditions emit very different amounts of SOA precursors. This reflects the poorly controlled (and thus highly variable) character of biomass combustion. This means that one likely cannot parameterize biomass burning SOA formation simply in terms of a specific fuel or perturbation type. Additional research is needed to quantify the full range of SOA precursors (not just the traditional precursors shown in Figure 8) in biomass burning emissions for a broad range of fuels and combustion conditions. However, perturbations of smoke from every fuel and burn condition studied showed extensive oxidation (even if there was no OA mass enhancement), confirming that biomass burning organic aerosol is highly chemically reactive and that the composition of biomass burning plumes will evolve rapidly due to atmospheric photochemistry.

Our results also suggest that ozone may be an important oxidant to drive SOA formation in biomass burning plumes. For example, Figure 4 shows that of all perturbations, ozone exposure produced, on average, the largest OA enhancement. This may be due, at least in part, to the relatively high ozone concentrations used in these experiments. However, ozone may be important for the nighttime processing of biomass burning plumes when other oxidants such as OH are less abundant. Field measurements of biomass smoke aging at night have rarely been performed—nocturnal studies are needed to determine the important of ozone-driven oxidation on SOA formation in real biomass burning plumes.

In this study, we conducted multiple experiments using the same fuel, same burn conditions, and same chamber conditions (e.g., seven experiments in which emissions from a black spruce fire were exposed to UV light and five experiments in which emissions from a ponderosa pine fire were exposed to UV light). The fact that these nominally identical experiments resulted in a wide variability in SOA production underscores the challenges associated with trying to draw conclusions from a single or small number of experiments.

References

Akagi, S. K., et al. (2012), Evolution of trace gases and particles emitted by a chaparral fire in California, *Atmos. Chem. Phys.*, *12*(3), 1397–1421, doi:10.5194/acp-12-1397-2012.

Akagi, S. K., et al. (2013), Measurements of reactive trace gases and variable O_3 formation rates in some South Carolina biomass burning plumes, *Atmos. Chem. Phys.*, *13*(3), 1141–1165, doi:10.5194/acp-13-1141-2013.

Andreae, M. O. (1990), Biomass burning in the tropics: Impact on environmental quality and global climate, *Popul. Dev. Rev.*, 268–291, doi:10.2307/2808077.

Bahreini, R., M. D. Keywood, N. L. Ng, V. Varutbangkul, S. Gao, R. C. Flagan, J. H. Seinfeld, D. R. Worsnop, and J. L. Jimenez (2005), Measurements of secondary organic aerosol from oxidation of cycloalkenes, terpenes, and m-xylene using an Aerodyne Aerosol Mass Spectrometer, *Environ. Sci. Technol.*, *39*(15), 5674–5688, doi:10.1021/es048061a.

Bernhammer, A.-K., M. Breitenlechner, F. N. Keutsch, and A. Hansel (2017), Technical note: Conversion of isoprene hydroxy hydroperoxides (ISOPOOHs) on metal environmental simulation chamber walls, *Atmos. Chem. Phys.*, *17*(6), 4053–4062, doi:10.5194/acp-17-4053-2017.

Bruns, E. A., I. El Haddad, J. G. Slowik, D. Kilic, F. Klein, U. Baltensperger, and A. S. H. Prévôt (2016), Identification of significant precursor gases of secondary organic aerosols from residential wood combustion, *Sci. Rep.*, *6*, 27,881.

Chan, A. W. H., K. E. Kautzman, P. S. Chhabra, J. D. Surratt, M. N. Chan, J. D. Crounse, A. Kürten, P. O. Wennberg, R. C. Flagan, and J. H. Seinfeld (2009), Secondary organic aerosol formation from photooxidation of naphthalene and alkylnaphthalenes: Implications for oxidation of intermediate volatility organic compounds (IVOCs), *Atmos. Chem. Phys.*, *9*(9), 3049–3060, doi:10.5194/acp-9-3049-2009.

Christian, T. J., B. Kleiss, R. J. Yokelson, R. Holzinger, P. J. Crutzen, W. M. Hao, B. H. Saharjo, and D. E. Ward (2003), Comprehensive laboratory measurements of biomass-burning emissions: 1. Emissions from Indonesian, African, and other fuels, *J. Geophys. Res.*, *108*(D23), 4719, doi:10.1029/2003JD003704.

Chuang, W. K., and N. M. Donahue (2016), A two-dimensional volatility basis set—Part 3: Prognostic modeling and NO_x dependence, *Atmos. Chem. Phys.*, *16*(1), 123–134, doi:10.5194/acp-16-123-2016.

Coggon, M. M., et al. (2016), Emissions of nitrogen-containing organic compounds from the burning of herbaceous and arboraceous biomass: Fuel composition dependence and the variability of commonly used nitrile tracers, *Geophys. Res. Lett.*, *43*, 9903–9912, doi:10.1002/2016GL070562.

Cubison, M. J., et al. (2011), Effects of aging on organic aerosol from open biomass burning smoke in aircraft and laboratory studies, *Atmos. Chem. Phys.*, *11*(23), 12,049–12,064, doi:10.5194/acp-11-12049-2011.

DeCarlo, P. F., et al. (2010), Investigation of the sources and processing of organic aerosol over the Central Mexican Plateau from aircraft measurements during MILAGRO, *Atmos. Chem. Phys.*, *10*(12), 5257–5280, doi:10.5194/acp-10-5257-2010.

De Gouw, J., and J. L. Jimenez (2009), Organic aerosols in the Earth's atmosphere, *Environ. Sci. Technol.*, *43*(20), 7614–7618, doi:10.1021/es9006004.

Farmer, D. K., A. Matsunaga, K. S. Docherty, J. D. Surratt, J. H. Seinfeld, P. J. Ziemann, and J. L. Jimenez (2010), Response of an aerosol mass spectrometer to organonitrates and organosulfates and implications for atmospheric chemistry, *Proc. Natl. Acad. Sci.*, *107*(15), 6670–6675, doi:10.1073/pnas.0912340107.

Grieshop, A. P., N. M. Donahue, and A. L. Robinson (2009), Laboratory investigation of photochemical oxidation of organic aerosol from wood fires 2: Analysis of aerosol mass spectrometer data, *Atmos. Chem. Phys.*, *9*(6), 2227–2240, doi:10.5194/acp-9-2227-2009.

Hallquist, M., et al. (2009), The formation, properties and impact of secondary organic aerosol: Current and emerging issues, *Atmos. Chem. Phys.*, *9*(14), 5155–5236, doi:10.5194/acp-9-5155-2009.

Hatch, L. E., W. Luo, J. F. Pankow, R. J. Yokelson, C. E. Stockwell, and K. C. Barsanti (2015), Identification and quantification of gaseous organic compounds emitted from biomass burning using two-dimensional gas chromatography-time-of-flight mass spectrometry, *Atmos. Chem. Phys.*, *15*(4), 1865–1899, doi:10.5194/acp-15-1865-2015.

Hawkins, L. N., and L. M. Russell (2010), Oxidation of ketone groups in transported biomass burning aerosol from the 2008 Northern California lightning series fires, *Atmos. Environ.*, *44*(34), 4142–4154, doi:10.1016/j.atmosenv.2010.07.036.

Hennigan, C. J., et al. (2011), Chemical and physical transformations of organic aerosol from the photo-oxidation of open biomass burning emissions in an environmental chamber, *Atmos. Chem. Phys.*, *11*(15), 7669–7686, doi:10.5194/acp-11-7669-2011.

Hurley, M. D., O. Sokolov, T. J. Wallington, H. Takekawa, M. Karasawa, B. Klotz, I. Barnes, and K. H. Becker (2001), Organic aerosol formation during the atmospheric degradation of toluene, *Environ. Sci. Technol.*, *35*(7), 1358–1366, doi:10.1021/es0013733.

Jolleys, M. D., et al. (2012), Characterizing the aging of biomass burning organic aerosol by use of mixing ratios: A meta-analysis of four regions, *Environ. Sci. Technol.*, *46*(24), 13,093–13,102, doi:10.1021/es302386v.

Jolleys, M. D., et al. (2015), Properties and evolution of biomass burning organic aerosol from Canadian boreal forest fires, *Atmos. Chem. Phys.*, *15*(6), 3077–3095, doi:10.5194/acp-15-3077-2015.

Kroll, J. H., and J. H. Seinfeld (2008), Chemistry of secondary organic aerosol: Formation and evolution of low-volatility organics in the atmosphere, *Atmos. Environ.*, *42*(16), 3593–3624, doi:10.1016/j.atmosenv.2008.01.003.

Lee, S., et al. (2008), Diagnosis of aged prescribed burning plumes impacting an urban area, *Environ. Sci. Technol.*, *42*(5), 1438–1444, doi:10.1021/es7023059.

Lim, Y. B., and P. J. Ziemann (2005), Products and mechanism of secondary organic aerosol formation from reactions of n-alkanes with OH radicals in the presence of NO_x, *Environ. Sci. Technol.*, *39*(23), 9229–9236, doi:10.1021/es051447g.

May, A. A., et al. (2013), Gas- and particle-phase primary emissions from in-use, on-road gasoline and diesel vehicles, *Atmos. Environ.*, *88*, 247–260.

McMeeking, G. R., et al. (2009), Emissions of trace gases and aerosols during the open combustion of biomass in the laboratory, *J. Geophys. Res.*, *114*, D19210, doi:10.1029/2009JD011836.

Miracolo, M. A., C. J. Hennigan, M. Ranjan, N. T. Nguyen, T. D. Gordon, E. M. Lipsky, A. A. Presto, N. M. Donahue, and A. L. Robinson (2011), Secondary aerosol formation from photochemical aging of aircraft exhaust in a smog chamber, *Atmos. Chem. Phys.*, *11*(9), 4135–4147, doi:10.5194/acp-11-4135-2011.

Ng, N. L., J. H. Kroll, A. W. H. Chan, P. S. Chhabra, R. C. Flagan, and J. H. Seinfeld (2007), Secondary organic aerosol formation from m-xylene, toluene, and benzene, *Atmos. Chem. Phys.*, *7*(14), 3909–3922, doi:10.5194/acp-7-3909-2007.

Ortega, A. M., D. A. Day, M. J. Cubison, W. H. Brune, D. Bon, J. A. de Gouw, and J. L. Jimenez (2013), Secondary organic aerosol formation and primary organic aerosol oxidation from biomass-burning smoke in a flow reactor during FLAME-3, *Atmos. Chem. Phys.*, *13*(22), 11,551–11,571, doi:10.5194/acp-13-11551-2013.

Parrington, M., et al. (2013), Ozone photochemistry in boreal biomass burning plumes, *Atmos. Chem. Phys.*, *13*(15), 7321–7341, doi:10.5194/acp-13-7321-2013.

Paulson, S. E., and J. J. Orlando (1996), The reactions of ozone with alkenes: An important source of HO_x in the boundary layer, *Geophys. Res. Lett.*, *23*(25), 3727–3730, doi:10.1029/96GL03477.

Reid, J. S., P. V. Hobbs, R. J. Ferek, D. R. Blake, J. V. Martins, M. R. Dunlap, and C. Liousse (1998), Physical, chemical, and optical properties of regional hazes dominated by smoke in Brazil, *J. Geophys. Res.*, *103*(D24), 32,059–32,080, doi:10.1029/98JD00458.

Rivera-Rios, J. C., et al. (2014), Conversion of hydroperoxides to carbonyls in field and laboratory instrumentation: Observational bias in diagnosing pristine versus anthropogenically controlled atmospheric chemistry, *Geophys. Res. Lett.*, *41*, 8645–8651, doi:10.1002/2014GL061919.

Robinson, A. L., N. M. Donahue, M. K. Shrivastava, E. A. Weitkamp, A. M. Sage, A. P. Grieshop, T. E. Lane, J. R. Pierce, and S. N. Pandis (2007), Rethinking organic aerosols: Semivolatile emissions and photochemical aging, *Science*, *315*(5816), 1259–1262.

Saleh, R., C. J. Hennigan, G. R. McMeeking, W. K. Chuang, E. S. Robinson, H. Coe, N. M. Donahue, and A. L. Robinson (2013), Absorptivity of brown carbon in fresh and photo-chemically aged biomass-burning emissions, *Atmos. Chem. Phys.*, *13*(15), 7683–7693, doi:10.5194/acp-13-7683-2013.

Simoneit, B. R. T., J. J. Schauer, C. G. Nolte, D. R. Oros, V. O. Elias, M. P. Fraser, W. F. Rogge, and G. R. Cass (1999), Levoglucosan, a tracer for cellulose in biomass burning and atmospheric particles, *Atmos. Environ.*, *33*(2), 173–182, doi:10.1016/S1352-2310(98)00145-9.

Simpson, I. J., J. J. Colman, A. L. Swanson, A. R. Bandy, D. C. Thornton, D. R. Blake, and F. S. Rowland (2001), Aircraft measurements of dimethyl sulfide (DMS) using a whole air sampling technique, *J. Atmos. Chem.*, *39*(2), 191–213, doi:10.1023/a:1010608529779.

Song, C., K. Na, and D. R. Cocker (2005), Impact of the hydrocarbon to NO_x ratio on secondary organic aerosol formation, *Environ. Sci. Technol.*, *39*(9), 3143–3149, doi:10.1021/es0493244.

Stockwell, C. E., P. R. Veres, J. Williams, and R. J. Yokelson (2015), Characterization of biomass burning emissions from cooking fires, peat, crop residue, and other fuels with high-resolution proton-transfer-reaction time-of-flight mass spectrometry, *Atmos. Chem. Phys.*, *15*(2), 845–865, doi:10.5194/acp-15-845-2015.

Weitkamp, E. A., A. M. Sage, J. R. Pierce, N. M. Donahue, and A. L. Robinson (2007), Organic aerosol formation from photochemical oxidation of diesel exhaust in a smog chamber, *Environ. Sci. Technol.*, *41*(20), 6969–6975.

Volkamer, R., P. J. Ziemann, and M. J. Molina (2009), Secondary organic aerosol formation from acetylene (C_2H_2): Seed effect on SOA yields due to organic photochemistry in the aerosol aqueous phase, *Atmos. Chem. Phys.*, *9*(6), 1907–1928, doi:10.5194/acp-9-1907-2009.

Yokelson, R. J., D. W. T. Griffith, and D. E. Ward (1996), Open-path Fourier transform infrared studies of large-scale laboratory biomass fires, *J. Geophys. Res.*, *101*(D15), 21,067–21,080, doi:10.1029/96JD01800.

Yokelson, R. J., et al. (2009), Emissions from biomass burning in the Yucatan, *Atmos. Chem. Phys.*, *9*(15), 5785–5812, doi:10.5194/acp-9-5785-2009.

Yokelson, R. J., et al. (2013), Coupling field and laboratory measurements to estimate the emission factors of identified and unidentified trace gases for prescribed fires, *Atmos. Chem. Phys.*, *13*(1), 89–116, doi:10.5194/acp-13-89-2013.

Zhang, Q., et al. (2007), Ubiquity and dominance of oxygenated species in organic aerosols in anthropogenically-influenced Northern Hemisphere midlatitudes, *Geophys. Res. Lett.*, *34*, L13801, doi:10.1029/2007GL029979.